Available online www.jocpr.com

Journal of Chemical and Pharmaceutical Research, 2015, 7(2):213-230

Research Article

ISSN : 0975-7384
CODEN(USA) : JCPRC5

DFT analysis of vibrational spectra of 1,3-dihydro-7-nitro-5-phenyl-*2H*-1,4-benzodiazepin-2-one

S. Prasath[1], R. Arun Balaji[2] and R. Revathy[3]

[1]Aksheyaa Engineering College, Chengalput, Tamilnadu, India
[2]Veltech Dr. R. R. & Dr. S. R. Technical University, Avadi, Tamilnadu, India
[3]Rajiv Gandhi College of Engineering, Sriperumbudur, Tamilnadu, India

---

ABSTRACT

The fourier transform infrared and fourier transform raman spectra of 1,3-dihydro-7-nitro-5-phenyl-2h-1,4-benzodiazepin-2-one (abbreviated as 3d7nbp) are recorded in the regions 4000–400 and 4000–100 cm-1, respectively. The appropriate theoretical spectrograms for the ir and raman spectra of the title molecule are also constructed. The calculated results show that the predicted geometry can well reproduce the structural parameters. Predicted vibrational frequencies have been assigned and compared with experimental ir spectra and they supported each other. stability of the molecule arising from hyperconjugative interactions, charge delocalization and intramolecular hydrogen bond-like weak interaction has been analyzed using natural bond orbital (nbo) analysis by using b3lyp/6-31g(d,p) method. The results show that electron density (ed) in the σ and π*antibonding orbitals and second-order delocalization energies e (2) confirm the occurrence of intramolecular charge transfer (ict) within the molecule. The first order hyperpolarizability (βtotal) of this molecular system and related properties (β, μ, and δα) are calculated using hf/6-31g (d,p) and b3lyp/6-31g(d,p) methods based on the finite-field approach. on the basis of vibrational analyses, the thermodynamic properties of the title compound at different temperatures have been calculated, revealing the correlations between,* $C_{p,m}^0$, S_m^0 *and* H_0^m *vs. temperature.*

Keywords: Vibrational study, Hyperpolarizability, PES, MEP, NBO.

INTRODUCTION

Benzodiazepines are widespread compounds used for the treatment of mental disorders and are known as anxiolytic drugs [1]. Benzodiazepines have been widely used to provide anxiolytic and sedation in various clinical settings since over four decades ago [2]. Benzo-diazepine class drugs are extensively used in the pharmacotherapy of anxiety disorders throughout the world. Their well-established anxiolytic properties have been entailed by an activation of GABA system, which is the principal inhibitory neurotransmitter system in brain. Conformational and electronic properties of 21 benzodiazepines are calculated by using empirical energy and semiempirical molecular orbital methods [3]. Analysis of thermochemical properties of some anxiolytic drugs are studied by Monajjemi et al., [4]. Nitrazepam(3D7NBP) is a type of benzodiazepine drug and is marketed in English-speaking countries under the following brand names: Alodorm, Arem, Insoma, Mogadon, Nitrados, Nitrazadon, Ormodon, Paxadorm, Remnos, and Somnite. It is a hypnotic drug used in the treatment of moderate to severe insomnia which has sedative and motor impairing properties [5], as well as anxiolytic, amnestic, anticonvulsant, and skeletal muscle relaxant properties. A literature survey reveals that to the best of our knowledge no HF/DFT wave number and structural parameter calculation of 3D7NBPhas been reported so far. Therefore, the present investigation is undertaken to study the vibrational spectra of this molecule in detail and to identify the various normal modes with greater wave number accuracy. In addition highest occupied molecular orbital (HOMO), lowest unoccupied molecular orbital (LUMO) analysis and first-order hyperpolarizability of this nonlinear optics (NLO) active molecule have been

investigated by ab initio HF and DFT methods. . The calculated HOMO and LUMO energies show that charge transfer occurs in the title molecule. These calculations are valuable for providing insight into the vibration spectrum and molecular parameters. Finally, the thermodynamic properties of the optimized structures are obtained theoretically from the harmonic vibrations.

EXPERIMENTAL SECTION

A pure sample of 3D7NBP was procured from Sigma-Aldrich Chemical Company, St. Louis, MO, USA, and used as such for spectral measurements. The Fourier transform infrared (FT-IR) spectrum of this compound was recorded in the region 4000-400 cm^{-1} on a Brucker model IFS 66 V spectrophotometer using the KBr pellet technique. The spectrum was recorded at room temperature, with a spectral solution of 4.0 cm^{-1}. The FT-Raman spectrum of 3D7NBP was recorded using Nd-YAG laser in the region 4000-100 cm^{-1} on the same spectrophotometer equipped with FRA 106 FTR module accessory. The experimental and theoretically predicted FT-IR and FT-Raman spectra of 3D7NBP with their scaled frequencies using scaled factors for each mode are shown in Figs. 1 and 2 respectively for comparison.

3. COMPUTATIONAL DETAILS

The quantum chemical calculations have been performed using Gaussian 03W program [6]. Full geometry optimizations and frequency calculations of the fundamental vibrational frequencies of all possible 1,4-benzodiapazine derivatives have been carried out employing Hartree-Fock (RHF) [7-8] and density Functional theory (B3LYP) [9-10] with 6-31G(d,p) basis sets [11]. Two different quantum chemical methods have been chosen due to the hydrogen bonding network governed in considered drugs and the satisfactory experimental correlations with the IR spectral frequencies. The absence of imaginary values of frequencies on the calculated vibrational spectrum conforms that the structure deduced corresponds to minimum energy. The assignments of the calculated frequencies are aided by the animation option of chemcraft program [12]. The DFT values are found to be in good agreement with the experimental values after scaling the vibrational frequencies in comparison to the RHF values. It should be noted that Gaussian 03 package does not calculate the Raman intensity. The recorded spectrum is in Raman intensity and computed is Raman activity; since we are comparing experimental with theoretical spectra we are converting the Raman activity into relative Raman intensities. The Raman activities are transformed into Raman intensities using RaInt program [13] by the expression:

$$I_i = 10^{-12} (n_o - n_i)^4 (1/n_i). S \quad (1)$$

Where $I_i$is the Raman intensity, S is the Raman scattering activities, n_i is the wavenumber of normal modes, and n_o denotes the wavenumber of the excitation laser [14]. Next, the spectra are analyzed in terms of the potential energy distribution (PED) contributions by using the Vibrational Energy Distribution Analysis program [15]. The mean linear hyperpolarizability and mean first hyperpolarizability properties of the title compound are obtained molecularpolarizabilities based on theoretical calculations.

RESULTS AND DISCUSSION

4.1. Molecular geometry

The numbering system adopted in the molecular structure of 3D7NBP is shown in Fig. 3.The optimized geometrical parameters, namely, bond lengths and angles calculated by both HF and B3LYP methods with 6-31G(d,p) basis set are listed in Table 1. Table 1 compares the calculated bond length and bond angles for 3D7NBP with those of experimental data [16]. A general priority for reproducing the experimental bond length is not present among HF and DFTeB3LYP levels. However, all the bond lengths and bond angles computed with the DFT - B3LYP levels show excellent agreement with available experimental results compared with HF levels.

6.4.2. Analysis of Vibrational frequencies

Vibrational frequency calculations, in general, are generally separated into two tasks:
(1) The calculations of the vibrational modes and frequencies.
(2) The calculations of the corresponding thermochemical parameters.

The vibrational analysis of 3D7NBP was performed on the basis of the characteristic vibrations of carbonyl, hydroxyl, nitro and phenyl ring modes. Theoretical calculations are performed using density functional theory (HF and B3LYP) with 6-31G (d, p) basis set. The title molecules are nonplanar and belong to C_1 point group. For C_1 symmetry there would not be any relevant distribution. In the present study we have followed two different scaling factors. HF/6-31G (d, p): 0.9181 and B3LYP/6-31G (d, p): 0.9608 [17].

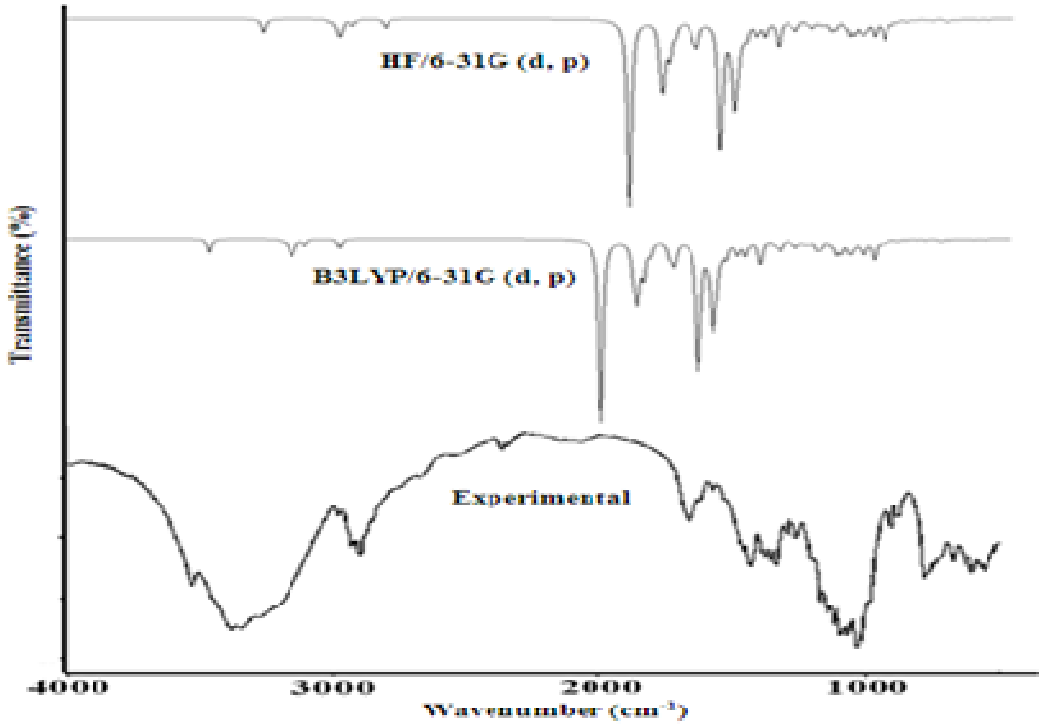

Fig.1. Experimental and calculated FTIR spectrum of 3D7NBP

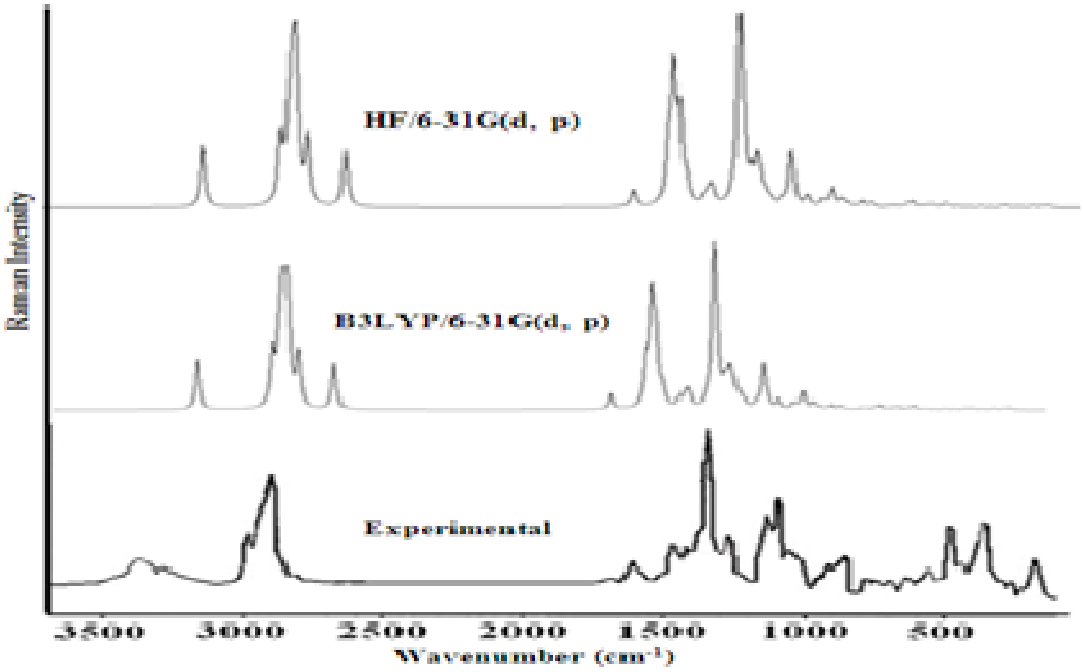

Fig.2. Experimental and calculated FT Raman spectrum of 3D7NBP

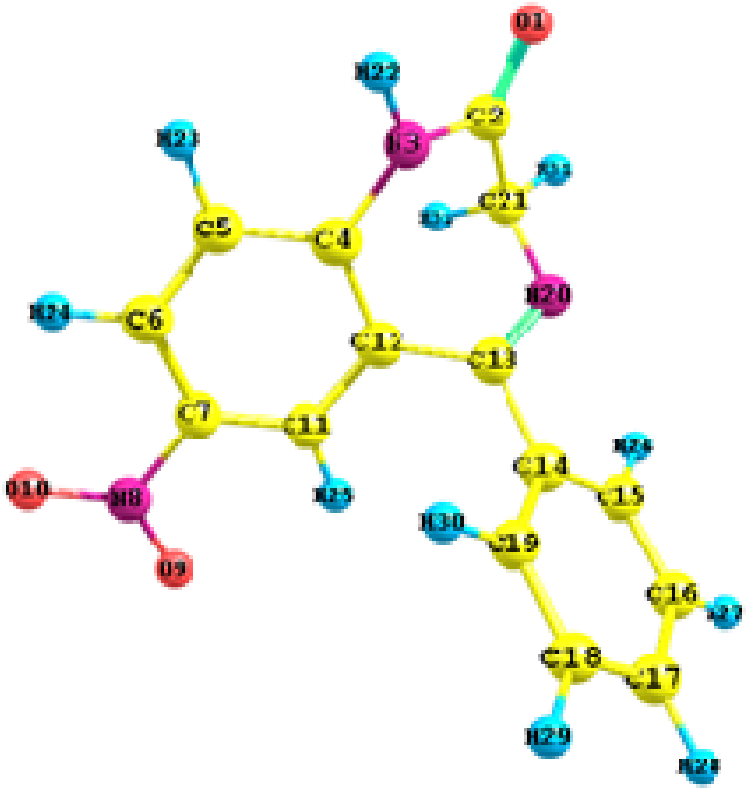

Fig.3. Atom numbering system adopted in this study for 3D7NBP

4.2.1. C–H vibrations

The hetero aromatic structure shows the presence of C–H stretching vibrations in the region 3200–3000 cm^{-1} which is characteristic region for the ready identification of C–H stretching vibrations [18]. Hetero cyclic compound C–H vibration absorption bands are usually weak, in many cases it is too weak for detection. In this region, the bands are not affected, appreciably by the nature of substituents. In the present work, the C-H vibrations are reported in mode no's 80 – 89 with a PED contribution ranging from 92 to 97%. Out of 4 modes reported, the wavenumbers of 3 modes viz 80,84,87 and 89 correlates well with the experimental values of FTIR (2966 cm^{-1}, 3133 cm^{-1} , 3169 cm^{-1},3178 cm^{-1}) and FTRaman (2941 cm^{-1}, 3139 cm^{-1} , 3166 cm^{-1},3185 cm^{-1}) which are listed in Table 2. The in-plane C–H bending vibrations normally appear in the range 1000–1300 cm^{-1} in the substituted benzenes and the out-of-plane bending vibrations occur in the region 750–1000 cm^{-1}region [19, 20]. In this study, the C–H in-plane-bending vibrations are assigned to 1498 cm^{-1}, 1171 cm^{-1} in FT-Raman and 1507 cm^{-1}, 1175 cm^{-1} in FT-IR. The C–H out-of-plane bending vibration is observed at 910 and 915 cm^{-1}in FT-Raman and FTIR respectively with a PED contribution of 84%.

4.2.2. C=O Vibrations

The C=O stretch of carboxylic acids is identical to the C=O stretch in ketones, which is expected in the region 1740-1660 cm^{-1} [21]. This band is reasonably easy to be recognized due to its high intensity [22]. In this study, the band observed at 1779 and 1772 cm^{-1} in FT-IR and FT-Raman spectra (mode No. 79) has been assigned to C=O stretching vibration, with the contribution of 85% PED. The calculated frequencies are slightly lesser than the observed values in the C=O stretching vibration.

4.2.3. N-H Vibrations

Primary aliphatic amines absorb in the region of 3450-3250 cm^{-1} in solid (or) liquids and their bands are broad and of medium intensity. In solid and liquid phases, a band of medium Intensity is observed in the range of 3400-3300 cm^{-1} for secondary aromatic amines. The vibrational bands due to the N-H stretching are sharp and weak than those of O-H stretching vibrations by virtue of which they can be easily identified. By observing the position of the band in the proper region, the vibrational band present at 3306 cm^{-1} as a medium band in FTIR and weak band cm^{-1} in FT Raman is assigned as N-H stretching vibration. The theoretically calculated values of N-H stretching vibrations (mode no: 90) are presented to be 3503 and 3582 cm^{-1} [B3LYP/6-31G (d, p) and HF/6-31G (d, p)] respectively.

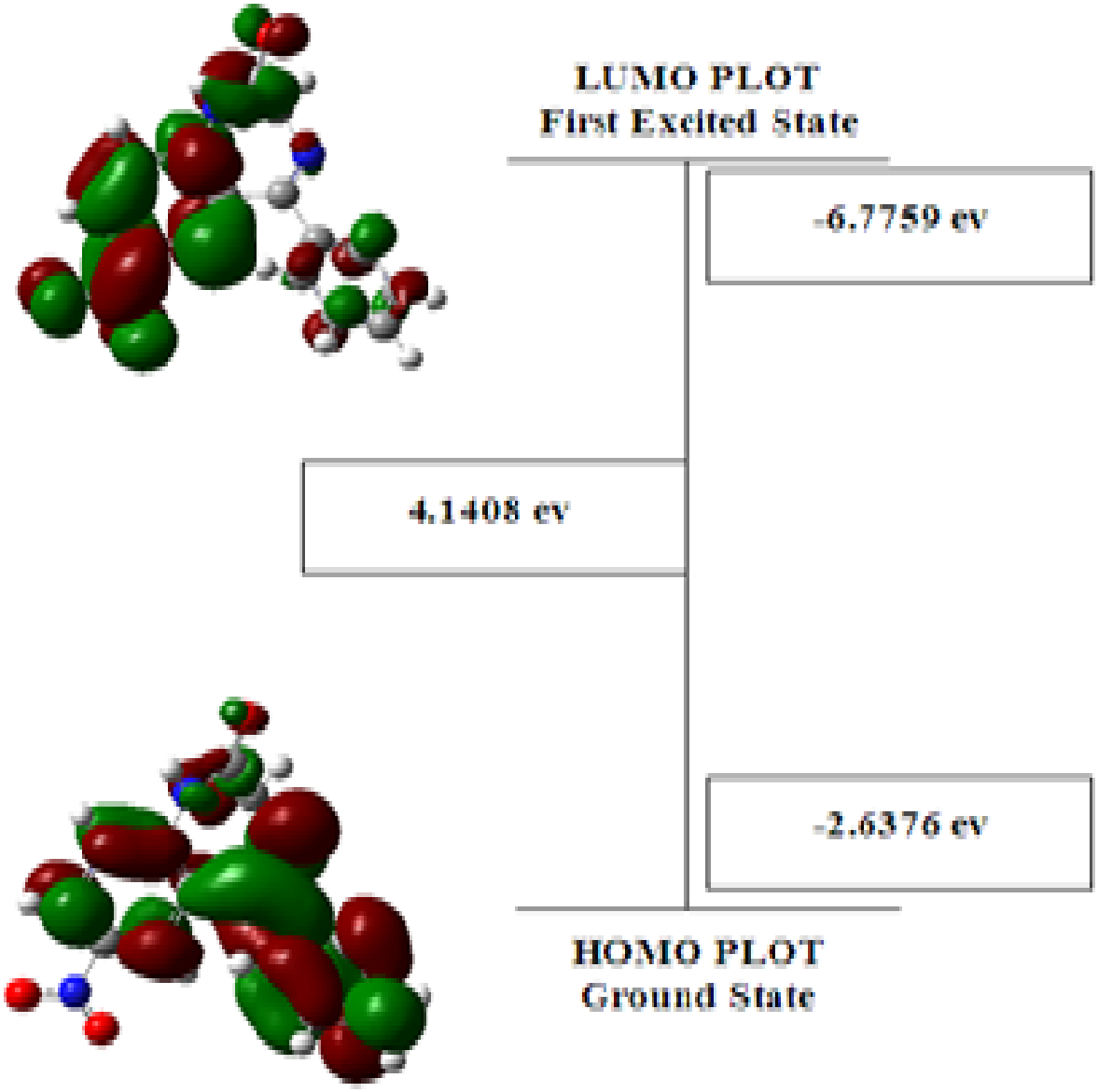

Fig.4. The HOMO and LUMO orbitals of 3D7NBP at B3LYP/6-31G(d,p)

4.2.4. C- N vibrations

The identification of C-N vibration is a very difficult task, since the mixing of several bands is possible in the region. Silverstein et al. [23] assigned C-N stretching absorption in the region 1342-1266 cm^{-1} for aromatic amines. In this study, the bands identified at 1299, 1296, 1188 and 1034 cm^{-1} in FT-IR spectra and at 1305, 1290, 1179 and1038 cm^{-1} in FT- Raman spectra have been assigned to C-N stretching vibrations. The theoretically scaled wave numbers at 1300,1286,1199, 1029 cm^{-1} by B3LYP/6-31G (d,p) method and 1271,1256,1174, 1026 cm^{-1} by HF/6-31G (d,p) method (mode nos. 61, 60, 57 and 49) corresponds to C-N stretching vibrations with PED of 30,19, 49, and 50%, respectively.

4.3. Hyperpolarizability

NLO effects arise from the interactions of electromagnetic fields in various media to produce new fields altered in phase, frequency, amplitude or other propagation characteristics' from the incident fields [24]. NLO is at the forefront of current research because of its importance in providing the key functions of frequency shifting, optical modulation, optical switching, optical logic, and optical memory for the emerging technologies in areas such as telecommunications, signal processing, and optical interconnections [25– 28]. The non-linear optical response of an isolated molecule in an electric field Ei (ω) can be represented as a Taylor series expansion of the total dipole moment, μ_{tot}, induced by the field:

$$\mu_{tot} = (\mu^2_x + \mu^2_y + \mu^2_z)^{1/2} \quad (2)$$

$$\alpha_0 = \frac{1}{3}(\alpha_{xx} + \alpha_{yy} + \alpha_{zz}) \quad (3)$$

$$\Delta\alpha = 2^{-1/2}\,[(\alpha_{xx} - \alpha_{yy})^2 + (\alpha_{yy} - \alpha_{zz})^2 + (\alpha_{zz} - \alpha_{xx})^2 6\alpha^2_{xx}]^{1/2} \quad (4)$$

$$\beta_0 = (\beta^2_x + \beta^2_y + \beta^2_z)^{1/2} \quad (5)$$

and

$$\beta_x = \beta_{xxx} + \beta_{xyy} + \beta_{xzz} \quad (6)$$

$$\beta_y = \beta_{yyy} + \beta_{xxy} + \beta_{yzz} \quad (7)$$

$$\beta_z = \beta_{zzz} + \beta_{xxz} + \beta_{yyz}.. \quad (8)$$

The calculated hyperpolarizability values of 3D7NBP are given in Table 3. Urea is one of the prototypical molecules used in the study of the NLO properties of molecular systems and frequently used as a threshold value for comparative purposes. The computed first hyperpolarizability, βtot of 3D7NBP molecule are 54.92 x 10^{-31}cm^5/esu and 138.52 x 10^{-31} cm^5/esu in HF and B3LYP methods respectively whose magnitude is very higher than that of urea (β of urea is 3.7289 × 10^{-31} cm^5/esu). Thus, this molecule might serve as a prospective building block for nonlinear optical materials.

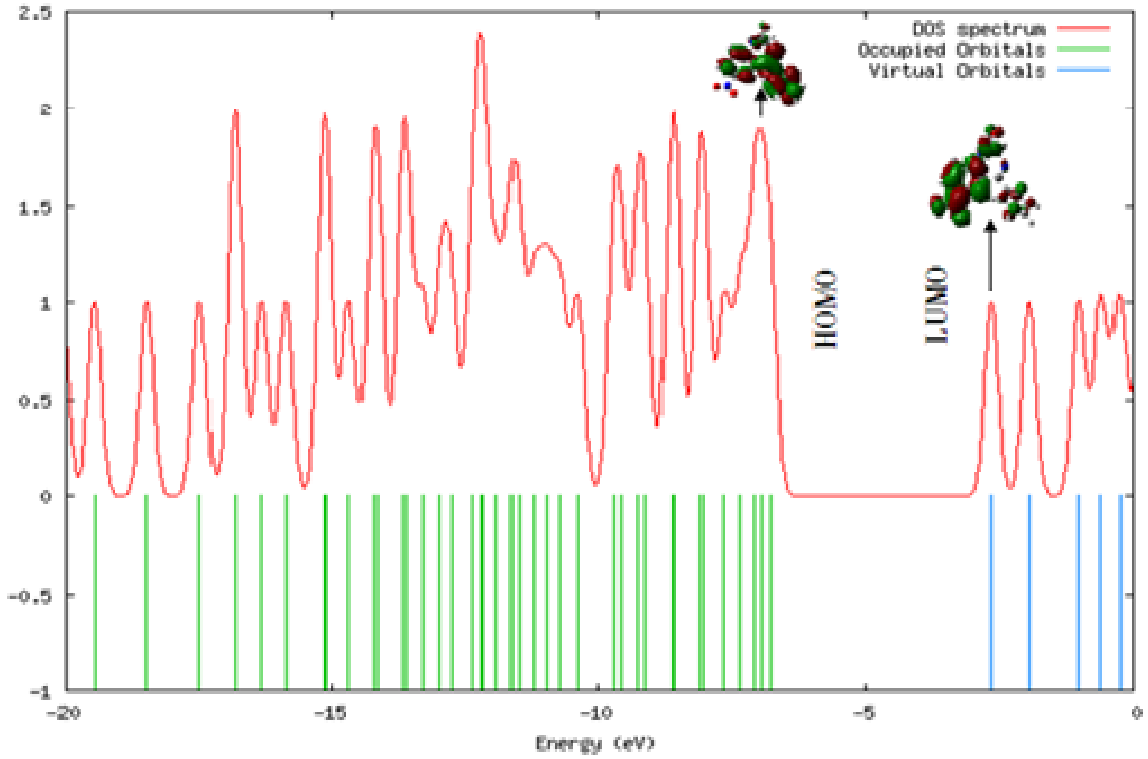

Fig.5. The calculated TDOS diagrams for 3D7NBP

4.4. HOMO–LUMO analysis

Many organic molecules, containing conjugated π electrons are characterized by large values of molecular first hyperpolarizabilities, are analyzed by means of vibrational spectroscopy [29-30]. In most cases, even in the absence of inversion symmetry, the strongest band in the FT Raman spectrum is weak in the FTIR spectrum and vice versa. But the intramolecular charge transfer from the donor to acceptor group through a single–double bond conjugated path can induce large variations of both the molecular dipole moment and the molecular polarizability, making FTIR and FT Raman activity strong at the same time. The experimental spectroscopic behavior described above is well accounted by ab initio calculations is π conjugated systems that predict exceptionally FTIR intensities for the same normal modes [30].

As DFT-based chemical reactivity description provides valuable information about the reactive sites for various types of attacks and orientation for benzidene [31], we have applied the same concepts during the studies. The Mulliken electronegativity (χ) [32], chemical hardness (η) and electronic potential are computed using the orbital energy of the HOMO (E_{HOMO}) and the orbital energy of the LUMO (E_{LUMO}) at the B3LYP/6-31G(d,p) and HF/6-

31G(d,p) levels of theory. The ionisation potential (μ) of the molecule is calculated using Koopmans's theorem [33-34] and is given by

$$\mu = \frac{E_{HOMO} + E_{LUMO}}{2} \quad (9)$$

$$\eta = \frac{E_{LUMO} - E_{HOMO}}{2} \quad (10)$$

Considering the chemical hardness, large HOMO–LUMO energy gap means a hard molecule and small HOMO–LUMO energy gap means a soft molecule. One can also relate the stability of the molecule to hardness, which means that the molecule with least HOMO–LUMO gap is more reactive. Table 6.4 lists the calculated values of the first Ionisation potentials, HOMO, LUMO and energy gaps of 3D7NBP.

The energy gap between the HOMO and the LUMO molecular orbitals is a critical parameter in determining molecular electrical transport properties because it is a measure of electron conductivity. The energy values of HOMO are computed as – 9.1371ev and - 6.7759evand LUMO are 1.3326ev and -2.6376ev for HF and B3LYP/6-31G (d,p) sets respectively. The energy gap value is 10.4697ev and 4.1408ev respectively for HF and DFT levels. Lower value in the HOMO and LUMO energy gap explains the eventual charge transfer interactions taking place within the molecule. Surfaces for the frontier orbitals are drawn to understand the bonding scheme of present compound. The HOMO–LUMO energy gap of 3D7NBP calculated at the B3LYP/6-31G(d,p) level (Fig 6.4) reveals that the energy gap reflects the chemical activity of the molecule. LUMO molecular orbital as an electron acceptor represents the ability to obtain an electron, and HOMO molecular orbital represents the ability to donate an electron.

4.5. Total, partial, and overlap population density-of-states

In the boundary region, neighboring orbitals may show quasi degenerate energy levels. In such cases, consideration of only the HOMO and LUMO may not yield a realistic description of the frontier orbitals. For this reason, the total (TDOS), partial (PDOS), and overlap population (OPDOS or COOP (Crystal Orbital Overlap Population)) density of states [36–38], in terms of Mulliken population analysis are calculated and created by convoluting the molecular orbital information with Gaussian curves of unit height and full width at half maximum (FWHM) of 0.3eV by using the Gauss Sum 2.2 program [39]. The TDOS, PDOS and OPDOS of the 3D7NBPare plotted in Figs. 5– 7, respectively. They provide a pictorial representation of MO (molecule orbital) compositions and their contributions to chemical bonding. The most important application of the DOS plots is to demonstrate MO compositions and their contributions to the chemical bonding through the OPDOS plots which are also referred in the literature as COOP diagrams. The OPDOS shows the bonding, anti-bonding and nonbonding nature of the interaction of the two orbitals, atoms or groups. A positive value of the OPDOS indicates a bonding interaction (because of the positive overlap population), negative value means that there is an anti-bonding interaction (due to negative overlap population) and zero value indicates nonbonding interactions [40]. Additionally, the OPDOS diagrams allow us to determine and compare of the donor–acceptor properties of the ligands and ascertain the bonding, non-bonding.

The calculated total electronic density of states (TDOS) diagrams of the 3D7NBP is given in Fig. 6.5. The partial density of state plot (PDOS) mainly presents the composition of the fragment orbitals contributing to the molecular orbitals which is seen from Fig. 6.6. As seen from Fig. 6.4, HOMO orbitals are localized on the ring and their contributions are about 85%. The LUMO orbitals are localized on the ring (65%) of the compound.

4.6. Molecular electrostatic potential (MEP)

The molecular electrostatic potential V(r) that is created in the space around a molecule by its nuclei and electrons is well established as a guide to molecular reactive behavior. It is defined by:

$$V(r) = \sum Z_A / (R_A - r) - \int \rho (r') / (r' - r) \, d r' \quad (11)$$

in which ZA is the charge of nucleus A, located at RA, ρ (r') is the electronic density function for the molecule and r' is the dummy integration variable [41,42]. MEP is related to the electronic density and is a very useful descriptor in determining sites for electrophilic and nucleophilic reactions as well as hydrogen bonding interactions [43, 44]. Being a real physical property, V(r) can be determined experimentally by diffraction or by computational methods [45]. However, identification of reactivity patterns based on the MEP exhibits intrinsic drawbacks, since the MEP is obtained through the classical electrostatic potential [46]. Then it is not possible to determine sites for nucleophilic attack because the zones of positive potential are not necessarily expressing affinity for nucleophiles but the concentrated nature of the nuclear charges. Molecular electrostatic potential mapping is very useful in the investigation of the molecular structure with its physiochemical property relationships [47- 49].

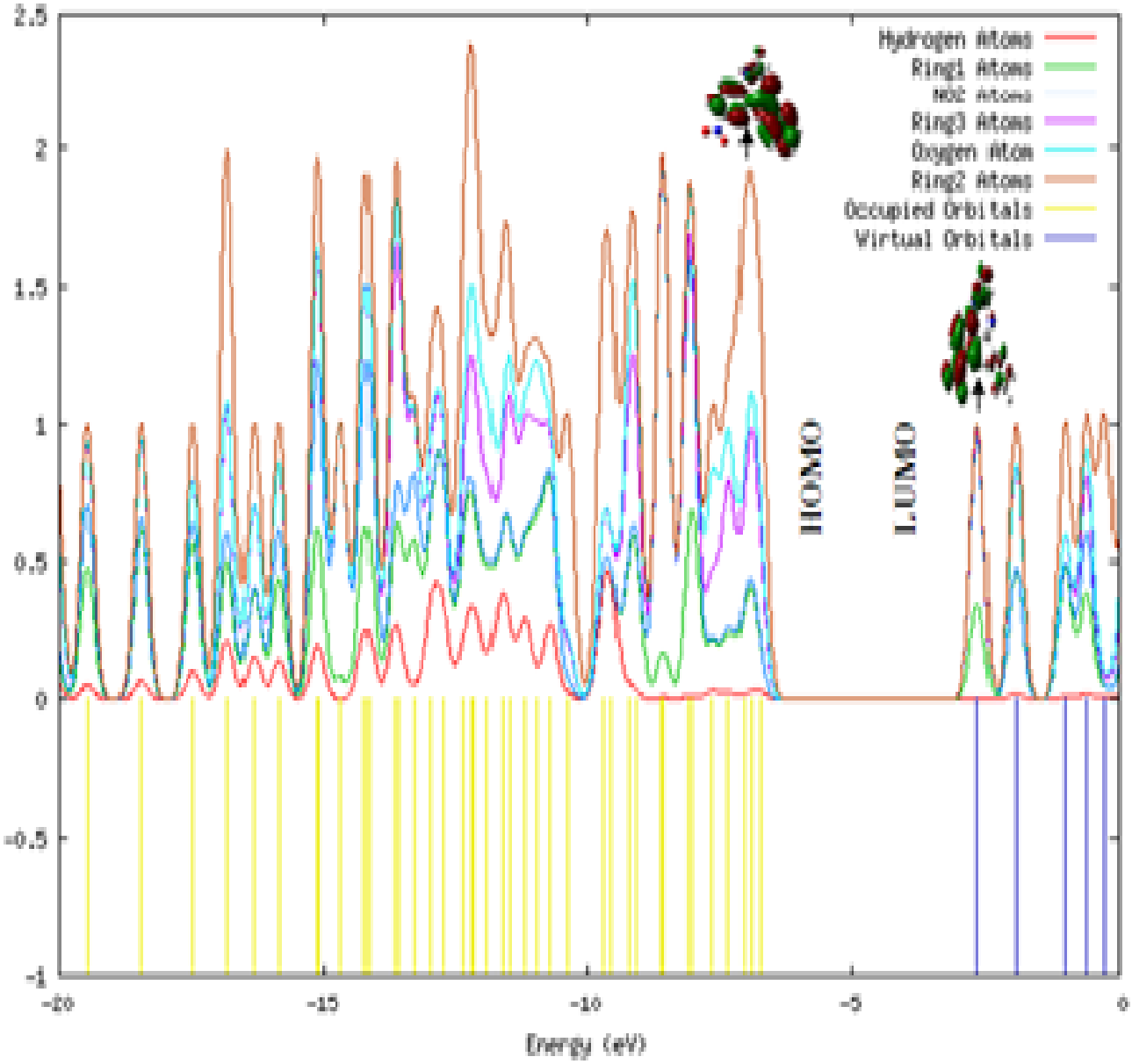

Fig.6. The calculated PDOS diagrams for 3D7NBP

As easily can be seen in Fig.8, this molecule has two possible sites for electrophilic attack. The different values of the electrostatic potential are represented by different colors. Potential increases in the order red<orange<yellow<green<blue. The color code of these maps in the range between -0.05 a.u. (deepest red) and 0.05 a.u.(white) in compound, where white indicates the strongest attraction (nucleophilic attack) and red indicates the strongest repulsion (electrophilic attack). The importance of MESP lies in the fact that it simultaneously displays molecular size, shape as well as positive, negative and neutral electrostatic potential regions in terms of colour grading and is very useful in research of molecular structure with its physiochemical property relationship [50-53].

4.7. Thermodynamic Properties

On the basis of vibrational analysis and statistical thermodynamic, the standard thermodynamic functions: heat capacity ($C^0_{p,m}$), entropy (S^0_m) and enthalpy (H^m_0) are calculated using perl script THERMO.PL [54] and are listed in Table 6.5. As observed from Table 6.5, the values of$C^0_{p,m}$, S^0_m and H^m_0, all increase of temperature from 100 to 1000 K there is an increment in all values, which is attributed to the enhancement of the molecular vibration as the temperature increases [55].

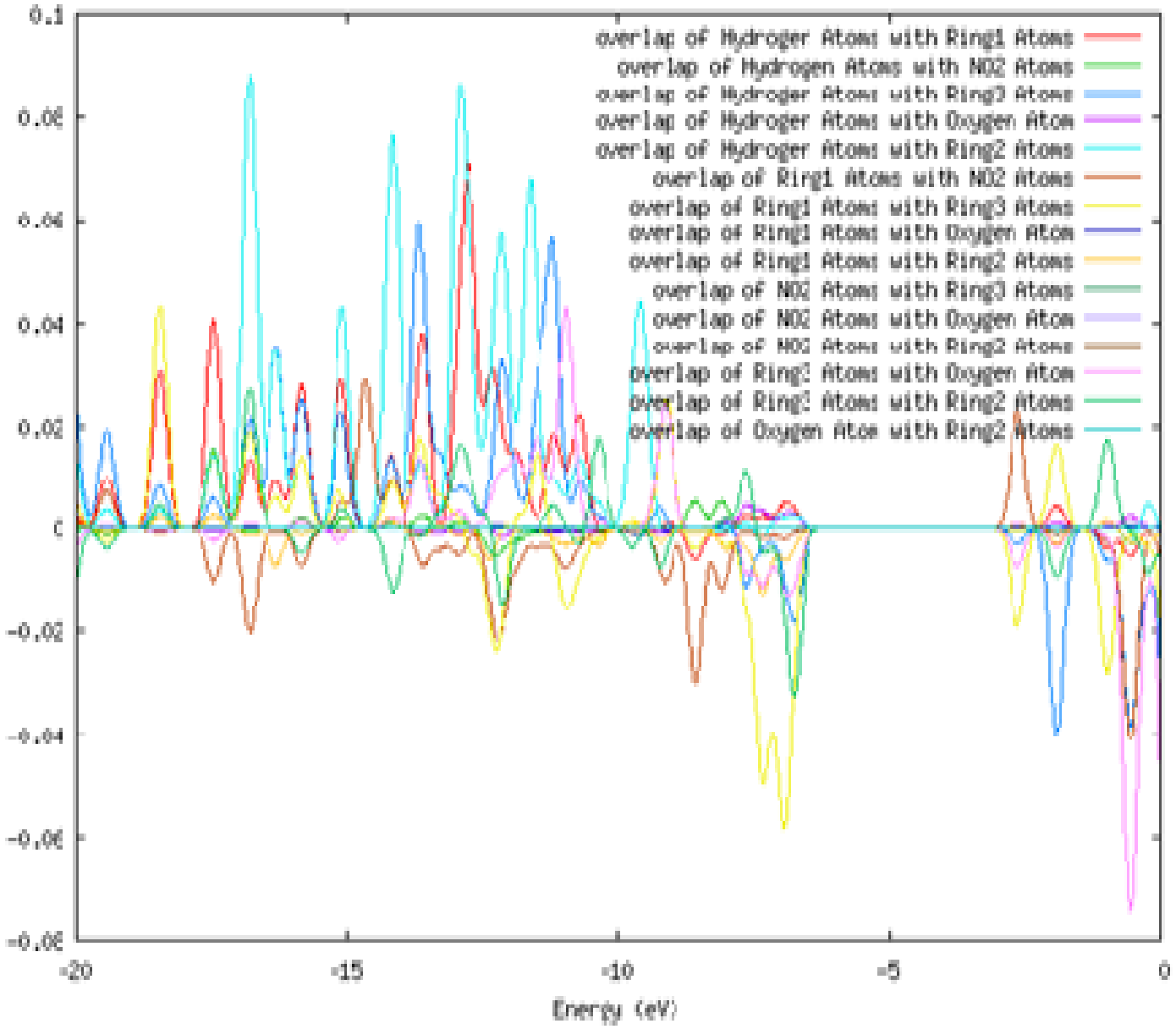

Fig.7. The OPDOS or COOP diagrams for 3D7NBP

The correlation equations between heat capacities, entropies, enthalpy changes and temperatures are fitted by quadratic formulas and the corresponding fitting factors (R^2) for these thermodynamic properties are 0.9991, 0.9999 and 0.9995, respectively. The corresponding fitting equations are as follows and the correlation graphics of that show in Fig 6.9.

$S_m^0 = 253.93 + 0.9791\ T - 18.9 \times 10^{-5} T^2$ ($R^2 = 0.9999$) (12)

$C_{p,m}^0 = 1.792 + 0.9799\ T - 38.7 \times 10^{-5} T^2$ ($R^2 = 0.9991$) (13)

$H_0^m = -9.493 + 0.097\ T + 28.1 \times 10^{-5} T^2$ ($R^2 = 0.9995$) (14)

All the thermodynamic data supply helpful information for the further study on 3D7NBP. They can be used to compute the other thermodynamic energies according to relationships of thermodynamic functions and estimate directions of chemical reactions according to the second law of thermodynamics in thermochemical field.

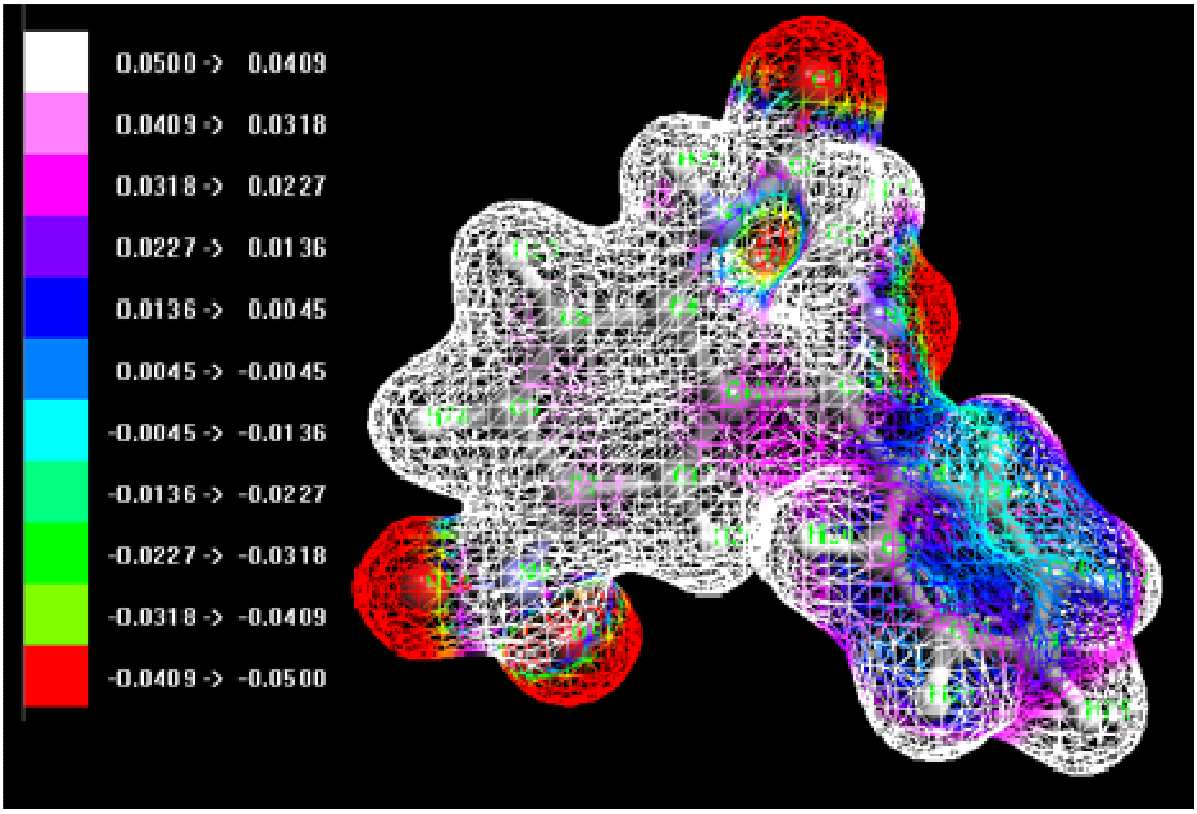

Fig.8.The total electron density surface mapped with electrostatic potential of 3D7NBP

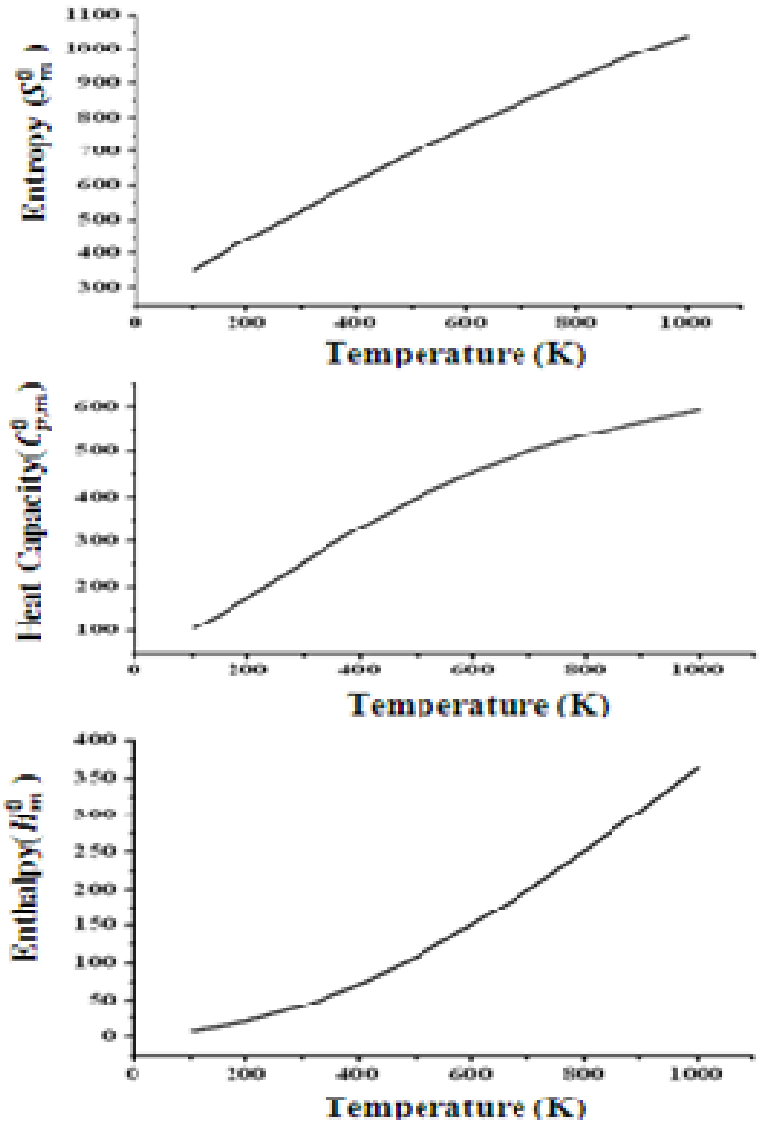

Fig.9. Correlation graphs of Thermodynamic properties at different temperatures for3D7NBP

Table.1. Optimized geometrical parameters of 3D7NBP molecules, bond length (Å), interfacial angles (º)

Parameters	Expt	HF/ 6-31G(d,p)	B3LYP/6-31G(d,p)
Bond length			
O_1-C_2	1.208	1.19	1.213
C_2-N_3	1.462	1.38	1.398
C_2-C_{21}	1.509	1.514	1.525
N_3-C_4	1.462	1.391	1.396
N_3-H_{22}	1.05	0.997	1.015
C_4-C_5	1.503	1.399	1.41
C_4-C_{12}	1.42	1.4	1.419
C_5-C_6	1.42	1.372	1.383
C_5-H_{23}	1.1	1.075	1.087
C_6-C_7	1.42	1.387	1.397
C_6-H_{24}	1.1	1.071	1.083
C_7-N_8	1.496	1.453	1.467
C_7-C_{11}	1.337	1.376	1.388
N_8-O_9	1.3	1.193	1.231
N_8-O_{10}	1.316	1.194	1.232
C_{11}-C_{12}	1.42	1.392	1.402
C_{11}-H_{25}	1.1	1.071	1.083
C_{12}-C_{13}	1.42	1.497	1.494
C_{13}-C_{14}	1.337	1.497	1.494

C_{13}-N_{20}	1.496	1.258	1.286
C_{14}-C_{15}	1.42	1.392	1.405
C_{14}-C_{19}	1.42	1.391	1.404
C_{15}-C_{16}	1.42	1.382	1.392
C_{15}-H_{26}	1.1	1.073	1.085
C_{16}-C_{17}	1.42	1.387	1.398
C_{16}-H_{27}	1.42	1.075	1.087
C_{17}-C_{18}	1.42	1.384	1.395
C_{17}-H_{28}	1.42	1.076	1.087
C_{18}-C_{19}	1.42	1.385	1.395
C_{18}-H_{29}	1.42	1.075	1.086
C_{19}-H_{30}	1.1	1.075	1.086
N_{20}-C_{21}	1.47	1.444	1.453
C_{21}-H_{31}	1.113	1.078	1.091
C_{21}-H_{32}	1.113	1.09	1.103
Bond angle			
O_1-C_2-N_3	122.6	120.5	120.6
O_1-C_2-C_{21}	122.5	124.1	124.9
N_3-C_2-C_{21}	118	115.4	114.5
C_2-N_3-C_4	103.85	126.9	127.5
C_2-N_3-H_{22}	118	112.9	112.4
C_2-C_{21}-N_{20}	120	111.3	111.3
C_2-C_{21}-H_{31}	108.8	106.9	106.9
C_2-C_{21}-H_{32}	108.8	108.6	108.3
C_4-N_3-H_{22}	118	117.2	117
N_3-C_4-C_5	120	117.9	118
N_3-C_4-C_{12}	120	122.1	122.1
C_5-C_4-C_{12}	120	119.9	119.8
C_4-C_5-C_6	120	120.9	121.2
C_4-C_5-H_{23}	120	119.2	119
C_4-C_{12}-C_{11}	120	118.6	118.2
C_4-C_{12}-C_{13}	120	121.9	122
C_6-C_5-H_{23}	120	119.8	119.8
C_5-C_6-C_7	120	118.7	118.5
C_5-C_6-H_{24}	120	121.2	121.7
C_7-C_6-H_{24}	120	120.1	119.8
C_6-C_7-N_8	120	119.2	119.2
C_6-C_7-C_{11}	120	121.5	121.5
N_8-C_7-C_{11}	120	119.3	119.2
C_7-N_8-O_9	120	117.8	117.8
C_7-N_8-O_{10}	120	117.5	117.5
C_7-C_{11}-C_{12}	120	120.3	120.6
C_7-C_{11}-H_{25}	120	119.4	119.1
O_9-N_8-O_{10}	120	124.8	124.7
C_{12}-C_{11}-H_{25}	120	120.2	120.3
C_{11}-C_{12}-C_{13}	120	119.6	119.7
C_{12}-C_{13} -C_{14}	120	118.1	118.4
C_{12}-C_{13} –N_{20}	120	124.4	124.6
C_{14}-C_{13} –N_{20}	120	117.5	117
C_{13}-C_{14}-C_{15}	120	119.3	119.2
C_{13}-C_{14}-C_{19}	120	121.7	122
C_{13}-N_{20}-C_{21}	120	120.5	119.5
C_{15}-C_{14}-C_{19}	120	119	118.8
C_{14}-C_{15}-C_{16}	120	120.4	120.6
C_{14}-C_{15}-H_{26} H_{2727}	120	119.1	118.6
C_{14}-C_{19}-C_{18}	120	120.5	120.6
C_{14}-C_{19}-H_{30}	120	120.2	120.1
C_{16}-C_{15}-H_{26}	120	120.5	120.9
C_{15}-C_{16}-C_{17}	120	120.2	120.2
C_{15}-C_{16}-H_{27}	120	119.8	119.7
C_{17}-C_{16}-H_{27}	120	120.1	120.1
C_{16}-C_{17}-C_{18}	120	119.8	119.7
C_{16}-C_{17}-H_{28}	120	120.1	120.1
C_{18}-C_{17}-H_{28}	120	120.1	120.1
C_{17}-C_{18}-C_{19}	120	120	120.1
C_{17}-C_{18}-H_{29}	120	120.2	120.2
C_{19}-C_{18}-H_{29}	120	119.7	119.7
C_{18}-C_{19}-H_{30}	120	119.3	119.3
N_{20}-C_{21}-H_{31}	120	109.1	109.3
N_{20}-C_{21}-H_{31}	120	112.1	112.1
H_{31}-C_{21}-H_{32}	109.4	108.7	108.7

Table.2. Calculated Scaled IR wavenumbers & relative intensities for 3D7NBP using HF/6-31G (d,p) & B3LYP/6-31G(d,p)

Species	Observed wavenumbers (cm^{-1})		Computed wavenumbers (cm^{-1})								Vibrational Assignments (PED, %)
			HF/6-31G(d,p)				B3LYP/6-31G(d,p)				
	FTIR	FT-Raman	Unscaled frequency	scaled frequency	IR intensity	Raman intensity	Unscaled frequency	scaled frequency	IR intensity	Raman intensity	
W(90)	3527	3525	3852	3482	10	44	3572	3503	7	35	ν NH (100)
W(89)	3178	3185	3425	3096	1	16	3256	3193	0	6	ν CH (93)
W(88)			3422	3093	0	51	3255	3192	1	30	ν CH (94)
W(87)	3169	3166	3393	3067	1	51	3229	3167	1	26	ν CH (92)
W(86)			3376	3052	3	100	3216	3153	3	48	ν CH (94)
W(85)			3366	3043	0	69	3207	3145	6	27	ν CH (96)
W(84)	3133	3139	3366	3043	6	12	3198	3136	1	27	ν CH (98)
W(83)			3355	3033	1	63	3197	3135	1	36	ν CH (96)
W(82)			3344	3023	0	22	3187	3126	0	12	ν CH (93)
W(81)	3085		3316	2997	3	66	3150	3089	3	37	ν CH (97)
W(80)	2967	2941	3170	2866	4	48	2996	2937	5	31	ν CH (97)
W(79)	1779	1772	2010	1817	100	12	1827	1791	100	10	ν CO (85)
W(78)	1682	1680	1903	1720	28	54	1684	1651	14	30	ν CN (63)
W(77)	1650	1645	1866	1687	69	2	1669	1637	29	11	ν NO (57)
W(76)	1620		1806	1633	0	60	1658	1626	4	67	ν CC (49)
W(75)			1798	1625	13	56	1640	1608	15	37	ν CC (42)
W(74)			1778	1607	0	3	1634	1603	2	10	ν CC (40)
W(73)	1573	1590	1768	1598	1	20	1612	1581	6	10	ν CC (68)
W(72)	1530	1544	1668	1508	0	5	1542	1512	0	4	ν CC (68)
W(71)	1507	1498	1662	1503	1	6	1527	1497	6	2	ρ CCH (52)
W(70)			1642	1484	5	5	1518	1488	3	5	ρ HCH (87)
W(69)	1469		1632	1475	12	23	1505	1476	11	10	ν CC (64)
W(68)	1455	1450	1627	1471	70	100	1493	1464	2	1	ν CC (71)
W(67)	1395		1606	1452	2	1	1423	1395	0	4	ν CC (72)
W(66)	1389	1377	1540	1392	1	1	1395	1368	65	100	ν NO (83)
W(65)	1359		1492	1349	18	3	1383	1356	12	31	ν CC (55)
W(64)	1341	1337	1468	1327	2	1	1368	1342	0	1	ν CC (82)
W(63)			1448	1309	27	11	1350	1324	3	5	ν CC (62)
W(62)	1315		1425	1288	10	18	1346	1320	3	10	ν CC (40)
W(61)	1299	1305	1406	1271	3	17	1326	1300	42	21	ν CN (30)
W(60)	1296	1290	1390	1256	6	6	1311	1286	16	11	ν CN (19)
W(59)	1250	1260	1341	1212	0	2	1288	1263	4	6	ν CC (59)
W(58)	1210		1331	1203	3	4	1267	1243	7	3	ν CC (55)
W(57)	1188	1179	1299	1174	0	2	1223	1199	6	2	ν CN (49)
W(56)			1291	1167	2	13	1216	1192	2	1	ν CC (82)
W(55)	1175	1171	1272	1150	3	22	1195	1172	0	3	ρ HCC (75)
W(54)	1167		1246	1126	2	4	1184	1161	7	29	ρ HCN (10)
W(53)	1142		1229	1111	6	4	1169	1146	1	3	ν CC (66)

Species	Observed wavenumbers (cm^{-1})		Computed wavenumbers (cm^{-1})								Vibrational Assignments (PED, %)
			HF/6-31G(d,p)				B3LYP/6-31G(d,p)				
	FTIR	FT-Raman	Unscaled frequency	scaled frequency	IR intensity	Raman intensity	Unscaled frequency	scaled frequency	IR intensity	Raman intensity	
W(52)	1115	1120	1213	1096	5	5	1122	1101	9	5	ν CC (33)
W(51)	1090	1095	1184	1070	0	0	1116	1094	6	1	ν CC (44)
W(50)	1057		1150	1040	3	3	1061	1040	1	4	ν CC (39)
W(49)	1034	1038	1135	1026	1	2	1049	1029	1	1	ν CN (50)
W(48)	1019	1025	1130	1022	0	0	1030	1010	5	1	ρ CNC (49)
W(47)	1004	1005	1122	1014	2	5	1018	998	0	11	ρ CCC (79)
W(46)	988		1115	1008	0	0	1003	984	0	0	t HCCC (82)
W(45)		962	1110	1003	0	0	981	962	0	0	t HCCN (62)
W(44)			1090	985	0	17	978	959	0	0	t HCCC (25)
W(43)			1086	982	1	2	976	957	1	4	t HCCC (12)
W(42)			1060	958	0	2	957	938	3	2	t HCCC (68)
W(41)	915	910	1049	948	3	10	945	927	1	1	γ HCCC (84)
W(40)	899		998	902	1	1	919	901	2	1	t HCCC (78)
W(39)			985	891	5	3	898	881	2	3	ρ ONO (12)
W(38)			960	867	1	1	865	848	3	1	t HCCC (48)
W(37)	838	853	958	866	3	2	863	846	2	2	t HCCN (13)
W(36)			933	843	5	1	843	827	4	1	ρ CCC (46)
W(35)	783	786	881	797	2	1	802	786	2	0	t HCCC (68)
W(34)	778	776	859	777	8	2	779	763	7	1	ρ ONO (28)
W(33)	750		854	772	7	1	756	742	5	1	γ OCON (38)
W(32)	724	733	828	748	2	0	751	737	1	0	γ OCON (29)
W(31)	702	693	790	714	4	1	723	709	4	1	γ OCNC (12)
W(30)			774	700	6	1	710	696	4	1	t CCCC (78)
W(29)			754	682	1	6	697	683	2	3	ρ CCC (13)
W(28)	669		729	659	2	1	668	655	2	0	t CCCC (19)
W(27)			706	638	3	1	659	646	6	1	ρ CCC (41)
W(26)	631	637	677	612	0	3	633	621	0	1	ρ CCC (80)
W(25)	604		642	580	9	2	611	599	10	2	t HNCC (47)
W(24)	566		621	562	6	1	579	568	2	1	ρ CNC (26)
W(23)	551	550	604	546	1	2	557	546	1	2	ρ CNC (16)
W(22)	516		593	536	1	1	548	537	1	1	ρ CCC (27)
W(21)	508	496	563	509	0	0	517	507	0	0	γ NCCC (28)
W(20)			544	492	1	1	500	491	1	1	ρ OCN (34)
W(19)		470	505	457	0	1	467	458	0	0	ρ CCC (33)
W(18)	448	431	487	441	0	0	449	440	0	0	ρ NCC (11)
W(17)			457	413	0	1	419	411	0	1	t CCCC (41)
W(16)			450	407	0	1	417	409	0	0	t CCCC (39)
W(15)		360	412	372	1	1	380	373	1	1	ρ CNC (17)
W(14)			358	323	0	2	331	325	0	1	ρ CCC (14)
W(13)		313	343	310	1	1	314	308	1	1	ν CN (26)

Species	Observed wavenumbers (cm^{-1})		Computed wavenumbers (cm^{-1})								Vibrational Assignments (PED, %)
			HF/6-31G(d,p)				B3LYP/6-31G(d,p)				
	FTIR	FT-Raman	Unscaled frequency	scaled frequency	IR intensity	Raman intensity	Unscaled frequency	scaled frequency	IR intensity	Raman intensity	
W(12)		305	333	301	0	1	307	301	0	1	ν CN (13)
W(11)			292	264	1	1	270	264	1	1	ρ CCN (25)
W(10)		252	269	244	0	1	253	248	0	0	ρ CCC (25)
W(9)		202	226	204	0	2	211	207	0	1	ρ CCC (35)
W(8)		176	186	168	0	2	171	167	0	1	ρ CCC (63)
W(7)			156	141	0	2	146	143	0	1	t CCCC (28)
W(6)			126	113	1	0	118	115	1	0	t CCCC (27)
W(5)			87	78	0	1	84	82	0	0	t ONCC (68)
W(4)			71	64	1	1	66	65	0	1	γ CCCC (52)
W(3)			56	51	0	5	53	52	0	2	γ CCCC (82)
W(2)			50	45	0	3	52	51	0	2	t CCCC (82)
W(1)			44	39	0	2	41	40	0	1	t CCCC (61)

υ – Stretching; γ – out of plane bending; ρ – in plane bending; t – torsion.

Table.3. The ab initio HF and B3LYP/6-31G (d, p) calculated μ, α and βfor 3D7NBP

Parameters	HF	B3LYP	Parameters	HF	B3LYP
μ_x	-1.3273	-1.1454	β_{xxx}	-32.073	323.174
μ_y	-1.1808	-0.7285	β_{xxy}	-63.059	-258.09
μ_z	-2.3423	-2.2719	β_{xyy}	452.7	802.265
μ (D)	2.9398	2.6465	β_{yyy}	-457.8	-948.545
α_{xx}	201.80	225.704	β_{xxz}	82.503	63.398
α_{xy}	-4.216	-7.618	β_{xyz}	-60.374	-45.411
α_{yy}	215.10	237.076	β_{yyz}	42.927	38.923
α_{xz}	-3.797	-4.1034	β_{xzz}	-4.022	2.0986
α_{yz}	-0.786	-0.7332	β_{yzz}	57.247	70.593
α_{zz}	84.58	87.439	β_{zzz}	-0.345	-8.8454
$\alpha_{(a.u)}$	167.16	183.41	β_{tot} (esu)	54.92 x10^{-31}	138.52 x10^{-31}
Δα (a.u)	371.01	416.71			

Table.4. Comparison of HOMO, LUMO, energy gaps and ionisation potentials of 3D7NBP

Basis set	HF/6-31G(d,p)	B3LYP/6-31G(d,p)
E_{HOMO}	-9.1371	-6.7759
E_{LUMO}	1.3326	-2.6376
Chemical hardness (η)	5.2348	2.0692
Ionisation potential (μ)	-3.9023	-4.7068
Energy gap	10.4697	4.1408
The Mulliken electronegativity (χ)	-5.2348	-2.0692

Table.5. Thermodynamic properties for 3D7NBP obtained by B3LYP/6-31G (d,p) density functional calculations

T(K)	S_m^0 (J/mol K)	$C_{p,m}^0$(J/mol K)	H_m^0 (kJ/mol)
100	349.80	105.23	6.98
200	443.83	176.10	20.95
298.15	528.48	253.65	42.01
300	530.05	255.13	42.48
400	614.17	332.24	71.91
500	695.76	399.58	108.60
600	773.71	455.26	151.43
700	847.41	500.61	199.30
800	916.76	537.69	251.28
900	981.91	568.32	306.63
1000	1043.15	593.90	364.77

CONCLUSION

Attempts have been made in the present work for the proper wavenumber assignments for the compound D7NBP from the FT-IR and FT-Raman spectra. The equilibrium geometries and harmonic frequencies of 3D7NBP are determined and analyzed both at HF and DFT levels of theories utilizing 6-31G (d, p) basis set. The difference between observed and calculated wavenumber values of the most of the fundamental modes is very small. Any discrepancy noted between the observed and the calculated frequencies may be due to the fact that the calculations have been actually done on single molecules in the gaseous state contrary to the experimental values recorded in the presence of intermolecular interactions. Therefore, the assignment made at higher levels of theory with only reasonable deviations from the experimental values seems to be correct. The HOMO and LUMO energy gap explains the chemical activity in the molecule. MEP confirms the non-existence of intermolecular interactions within the molecule.

REFERENCES

[1] J.Dourlat, W.Q.Liu, N.Gresh, C.Garbay, *Bioorganic and Medicinal Chemistry Letters*. 17(**2007**) 2527-2530.
[2] A.Zarghi , A.Tabatabai , M.Faizi , A.Ahadian, P.Navabi , V.Zanganeh, *Bioorganic and Medicinal Chemistry Letters*. 15(**2005**) 1863–1865
[3] D.Berezhnoy, R.Baur, A.Gonthier, B.Foucaud, M.Goldner and E.Sigel, *j.Neurochem*, 92(**2005**), 859.
[4] M.Monajjemi, M.H.Razavian, F.Mollaamin , F.Naderi, B.Honarparvar, *African Journal of Pharmacy and Pharmacology*, 4(8) (**2010**) 521-529.

[5] M.Yasui,A.Kato, T.Kanemasa, S.Murata, K.Nishitomi, K.Koike, N.Tai, S.Shinohara, M.Tokomura, M.Horiuchi, K.Abe, Pharmacological profiles ofbenzodiazepinergic hypnotics and correlations with receptor subtypes,Nihon ShinkeiSeishin Yakurigaku Zasshi25 (3) (**2005**) 143–51.
[6] Gaussion 03 program, (Gaussian Inc.,Wallingford CT) **2004**.
[7] CCJ .Roothan, New developments in molecular orbital theory Rev. Mod. Phys,23 (**1951**) 69-89.
[8] J.A.Pople and R.K.Nesbet. *J. Chem. Phys*.22 (**1954**) 571- 572.
[9] A.D.Becke, *J.Chem. Phys*, 98 (**1993**) 1372 - 1377.
[10] C.Lee, W.Yang and R.G.Parr . *Phys. Rev. B*, 37 (**1998**) 785-789
[11] M.J.Frisch, J.A. Pople and J.E.Del Bene. *J. Phys. Chem*. 89 (**1985**) 3669-3674.
[12] G.A.Zhurko, D.A.Zhurko, Chemcraft program, Academic version 1.5, **2004**.
[13] D. Michalska, Raint Program, Wroclaw University of Technology, **2003**.
[14] D. Michalska, R. Wyokinski, Chem. Phys. Lett. 403 (**2005**) 211.
[15] M.H. Jamroz, Vibrational Energy Distribution Analysis VEDA 4 program, Warsaw,**2004**
[16]G. Gilli, V. Bertolasi, M. Sacerdoti and P. A. Borea, *Acta Cryst*. B34(**1978**) 3793 - 3795
[17]A.P.Scott and L.Radom . *J. Phys. Chem*.100 (**1996**) 16502-16513.
[18]G. Varsanyi, Assignments for Vibrational Spectra of Seven Hundred Benzene derivatives, 1/2 Academic Kiaclo, Budapest, **1973**.
[19] S. Muthu, J. Uma Maheswari, *Spectrochim. Acta Part* A 92 (**2012**) 154-163.
[20] D. Becke, *J. Chem. Phys*. 98 (**1993**) 5648–5652.
[21] D. Lin-Vien, N.B. Colthup, W.G. Fateley, J.G. Grasselli, The Handbook of Infrared and Raman Characteristic Frequencies of Organic Molecules, Academic Press, Boston, MA, **1991**.
[22] R. Meenakshi, J. Lakshmi, S. Gunasekaran, S. Srinivasan, *J. Mol. Simul*. 36 (**2010**) 425-433.
[23] M. Silverstein, G. Clayton Bassler, C. Morril, Spectroscopic Identification of Organic compounds, John Wiley, Newyork, **1981**.
[24] X. Sun, Q.L. Hao, W.X. Wei, Z.X. Yu, D.D. Lu, X. Wang, Y.S. Wang, *J. Mol. Struct. Theochem* 904 (**2009**) 74–82.
[25] C. Andraud, T. Brotin, F. Pelle, P. Goldner, B. Bigot, A. Collet, *J. Am. Chem. Soc*. 116 (**1994**) 2094–2102.
[26] V.M. Geskin, C. Lambert, J.L. Bredas, *J. Am. Chem. Soc*. 125 (**2003**) 15651–15662.
[27] M. Nakano, H. Fujita, M. Takahata, K. Yamaguchi, *J. Am. Chem. Soc*. 124 (**2002**) 9648–9655.
[28] D. Sajan, I.H. Joe, V.S. Jayakumar, J. Zaleski, *J. Mol. Struct*. 785 (**2006**) 43–53.
[29]**Y. Atalay**, D.Avcı, A. Başoğlu,*J. Structural Chemistry*., 19(**2008**) 239–246.
[30]T. Vijayakumar, I. Hubert Joe, C.P.R. Nair, V.S. Jayakumar, *J. Chemical Physics*., 343(**2008**) 83–99.
[31] R.G. Pearson, *J. Chem. Sci.,* 117(**2005**)369 - 377.
[32] S. Bavafa, *Asian J. Chemistry*., 22(**2010**) 5237 - 5243.
[33] T.A. Koopmans, *Physica*, 1(**1934**)104-113.
[34] J. Zevallo s and A. Toro-Labbe, *Journal of the Chilean Chemical Society*. 48(**2003**) 39-47.
[35] D.A. Prystupa, A. Anderson, and B.H. Torrie., *Journal of Raman Spectroscopy*, 25, (**1994**)175–182.
[36] R. Hoffmann, Solids and Surfaces: A Chemist's View of Bonding in Extended Structures, VCH Publishers., New York, **1988**.
[37] T. Hughbanks, R. Hoffmann, *J. Am. Chem. Soc*. 105 (**1983**) 3528–3537.
[38] J.G. Małecki, *Polyhedron* 29 (**2010**) 1973–1979.
[39] N.M. O'Boyle, A.L. Tenderholt, K.M. Langner, *J. Comp. Chem.* 29 (**2008**) 839–845.
[40] M. Chen, U.V. Waghmare, C.M. Friend, E. Kaxiras, *J. Chem. Phys*. 109 (**1998**) 6680–6854.
[41] P. Politzer, P.R. Laurence, K. Jayasuriya, *Environ. Health Perspect*.61 (**1985**) 191-202.
[42] P. Politzer, P. Lane, *Struct. Chem*. 1 (**1990**) 159-164.
[43] E. Scrocco, J. Tomasi, *Adv. Quantum Chem*. 11 (**1979**) 115-193.
[44] F.J. Luque, J.M. Lopez, M. Orozco, *Theor. Chem. Acc.* 103 (**2000**) 343-345.
[45] P. Politzer, D.G. Truhlar, Chemical Applications of Atomic and Molecular Electrostatic Potentials, Plenum Press, Newyork, **1981**.
[46] R.F.W. Bader, *Chem. Rev*. 91 (**1990**) 893-928.
[47] J.S. Murray, K. Sen, Molecular Electrostatic Potentials. Concepts and Applications, Elsevier, Amsterdam, **1996**.
[48] J.M. Seminario, Recent Development and Applications of Modern Density Functional Theory, Elsevier, 4 (**1996**) 800-806.
[49] T. Yesilkayanak, G. Binzet, F. Mehmet Emen, U. Florke, N. Kulcu, H. Arslan, *Eur. J. Chem.* 1 (**2010**) 1-5.

[50] C. Munoz-Caro, A. Nino, M.L. Sement, J.M. Leal, S. Ibeas, *Journal of Organic Chemistry*, 65 (**2000**) 405–410.
[51] P. Politzer, K.C. Daiker, The Force Concept in Chemistry, Van Nostrand Reinhold Co., **1981**.
[52] J.S. Politzer, Murray, D.L. Protein, R. Beveridge, Lavery (Eds.), Theoretical Biochemistry and Molecular Biophysics: A Comprehensive Survey, vol. 2, Adenine Press, Schenectady, NY, **1991**.
[53] E. Scrocco, J. Tomasi, Topics in Current Chemistry, vol. 42, Springer-Verlag, Berlin, **1973**.
[54] K. K. Irikura, THERMO. PL (National Institute of Standards and Technology, Gaithersburg, MD, **2002**).
[55]J. Bevan Ott, J. Boerio-Goates, Calculations from Statistical Thermodynamics, Academic Press, **2000**.